Magnetic ordering induced magnetostriction dynamics via pulsed magnetic field in the polar magnet $CaBaCo_4O_7$

Dequan Jiang,[1,*] Huakun Zuo,[1,*] Zhuo Zeng,[1] Haoyu Niu,[1] Youyuan Liang,[1] Hao Huang,[1] Peng Yang,[1] Zhuoda Dong,[1] Yu Sui,[2] Young Sun,[3] Zhongwen Ouyang,[1] and Zhengcai Xia[1,†]

[1]*Wuhan National High Magnetic Field Center and School of Physics, Huazhong University of Science and Technology, Wuhan 430074, People's Republic of China*

[2]*School of Physics, Harbin Institute of Technology, Harbin 150001, People's Republic of China*

[3]*Center of Quantum Materials and Devices and Department of Applied Physics, Chongqing University, Chongqing 401331, People's Republic of China*

(Received 11 September 2023; revised 17 December 2023; accepted 29 February 2024; published 18 March 2024)

The magnetization, magnetostriction, and electric polarization of $CaBaCo_4O_7$ single-crystal samples were investigated under static and pulsed magnetic fields. Experimental results show that the ferrimagnetic order and metamagnetic transition occur in a lower-temperature region. At 4.2 K, with the increase of the applied magnetic field, there is a transition from multidomain to single domain at about 2 T, and then with the further increase of the magnetic field, the spin of cobalt ions (Co1 and Co4 ions) changes from noncollinear to collinear. Along with this magnetization process, magnetostriction also exhibits two continuous processes: magnetostriction related to magnetic domain rotation and magnetostriction related to the increase of spin collinearity. Especially in pulsed magnetic fields, the magnetization, magnetostriction, and polarization transitions induced by magnetic order occur almost in the same critical magnetic field. We assume that in the system, the magnetic order can further polarize the orbital via spin-orbit interaction, resulting in strong magnetostriction.

DOI: 10.1103/PhysRevB.109.104418

I. INTRODUCTION

Multiferroic materials have attracted a great deal of attention due to their potential for a variety of application scenarios such as computer storage and sensors [1–3]. The realization of these functions, to a large extent, relies on magnetoelectric (ME) effects, i.e., magnetic field control of electric polarization and electric field control of magnetization [4,5]. The coupling between magnetization and electric polarization in multiferroic materials generates complex physical properties and novel application prospects [6]. Although the typical materials $BiFeO_3$ [7] and $TbMnO_3$ [8] are extensively reported, multiferroic materials are quite rare. In addition, the most pronounced ME effects were observed in ferroelectric and ferromagnetic composites, where the ferromagnetic component with large magnetostriction coefficients is a key component in producing large ME effects through interface elastic coupling [9,10]. Meanwhile, magnetostriction is often closely related to frustration. In frustrated magnets, such as $Ni_3V_2O_8$ [11,12], $MnWO_4$ [13], and $CuFeO_2$ [14], the competition between geometrical frustration and magnetic ordering leads to the emergence of peculiar magnetic properties and magnetic transitions. The magnetostriction of $CaBaCo_4O_7$ (CBCO) is responsible for the strong magnetoelectric coupling that occurs near the magnetic phase transition [15–17]. Even though this research in this area has been going on for decades, there still exist some mechanisms that are not fully understood.

It has been reported that there is a magnetic induced electric polarization of $\Delta P = 17\text{mC/m}^2$ in CBCO [18–22], and the dielectric constant is significantly modulated by the magnetic fields. When magnetic phase transition occurs at 15 T, the dielectric constant (ε) decreases by more than 15% [23–25]. Many theoretical calculations related to CBCO have been reported. Vienna *Ab Initio* Simulation Package calculations show that the large change in polarization observed in CBCO during the phase transition from pyroelectric paramagnetism to ferrimagnetism may be the result of the exchange striction effect [26]. In addition, it has been reported that Ni^{2+} doping on CBCO can enhance its antiferromagnetic interactions, which significantly increases its polarization and extends its temperature range [22]. Based on previous infrared and dielectric spectroscopy results, it has been demonstrated that there is a spin-lattice coupling in the $CaBaM_4O_7$ (M = Co, Fe) material family [27]. First-principles calculations suggest that the strong orthorhombic distortion in these materials may partially release geometrical frustration, leading to the appearance of ferrimagnetic order [28]. The orthorhombic distortion in CBCO may be caused by Jahn-Teller activity of Co^{3+} (in the $e_g^3 t_{2g}^3$ configuration) oxygen tetrahedra [29–31]. This speculation is supported by the fact that Co-O has different bond lengths at different Co sites at different temperatures [28].

Based on neutron diffraction and thermal expansion measurements, the transition from the paramagnetic to the ferrimagnetic phases in CBCO is accompanied by an abrupt

*These authors contributed equally to this work.
†Corresponding author: xia9020@hust.edu.cn

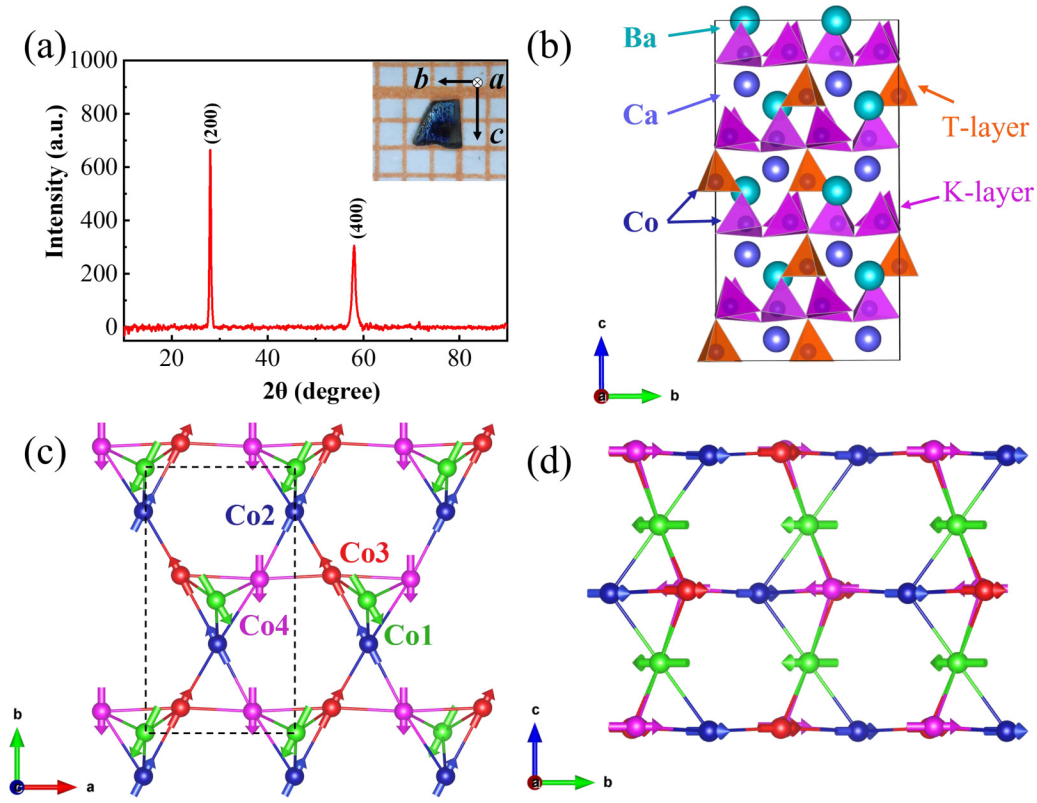

FIG. 1. (a) The XRD diffraction pattern of CBCO single crystal. The inset shows the image of the CBCO single-crystal sample. (b) The crystal structure of CBCO. It consists of a 1:1 stacking of kagome (K) and triangular (T) lattice layers of CoO_4 tetrahedra along the c axis. The Ba, Ca, and Co ions are shown with large, medium, and small balls, respectively. (c) and (d) are the schematic representations of the magnetic structure of CBCO along the [001] and [100] directions, respectively. The different Co sites are labeled by different colors and the spin directions are indicated with arrows.

drop in the lattice constant c, suggesting that the large ME effect may be related to exchange striction [32,33]. At zero magnetic field, there is still controversy about the properties of CBCO above T_C. From measurements of dielectric constant and specific heat, Caignaert *et al.* speculated that the anomaly at $T^* \sim 69$ K should not be attributed to a magnetic ordering [15]. Recent single-crystal neutron diffraction measurements have confirmed the occurrence of an antiferromagnetic transition in CBCO at T^* and have proposed the existence of an antiferromagnetic structure between T_C and T^*. Consequently, the larger ME response of CBCO may be associated with antiferromagnetic structure [16]. Previous studies in CBCO have focused on the discussion of lattice and magnetic phase transitions around the transition temperature $T_C \sim 62$ K [20]. To understand the intrinsic interaction between magnetization and lattice (electric polarization), the investigations of the spin-lattice coupling, especially at low temperatures, and their dynamic properties are necessary. In this paper, we report the experimental results of lower-temperature magnetization, magnetostriction, and polarization measurements with a multipulse magnet. The results show that there is strong spin-lattice coupling in CBCO single crystals, and the relaxation behavior of the lattice is tightly correlated with the deflection of twinned domains and noncollinear to collinear transition of Co1 and Co4 ions. Based on the exchange striction model, the lattice change of the Co-O-Co chain (along the c axis), and the local spin correlations, the dynamic coupling between magnetization and magnetostriction are discussed, which is helpful to understand the intrinsic spin-lattice coupling and their dynamic behaviors via pulsed magnetic fields.

II. EXPERIMENTAL DETAILS

Single crystals of CBCO were grown by a four-mirror optical floating zone furnace, and were confirmed to be single phase by monochromatic Cu $K\alpha$ radiation ($\lambda = 0.1542$ nm) x-ray diffraction (XRD; Bruker D2 phaser). The orientation of crystallographic axes is determined by single-crystal x-ray diffractometry, and the lattice parameters $a = 6.29$Å, $b = 11.01$Å, and $c = 10.19$Å are obtained at room temperature. Figure 1(a) shows the crystallographic direction along the a axis. Low-field magnetization measurements were carried out using a commercial superconducting quantum interference device magnetometer (Quantum Design) in the temperature range of 2–300 K. Static magnetic field magnetostriction ($\Delta L/L$) measurements were performed in a physical property measurement system (Quantum Design). The magnetostriction ($\Delta L/L$) was measured using resistance-type strain gauges (KFLB-05-120-C1-11, KYOWA) with a resolution of $(\Delta L/L) \sim 1 \times 10^{-5}$. In this paper, we focus on the magnetostriction $(\Delta L/L)_c$ measurements along the c axis and $(\Delta L/L)_b$ along the b axis.

High-field magnetization, magnetostriction, and electric polarization were measured at Wuhan National High

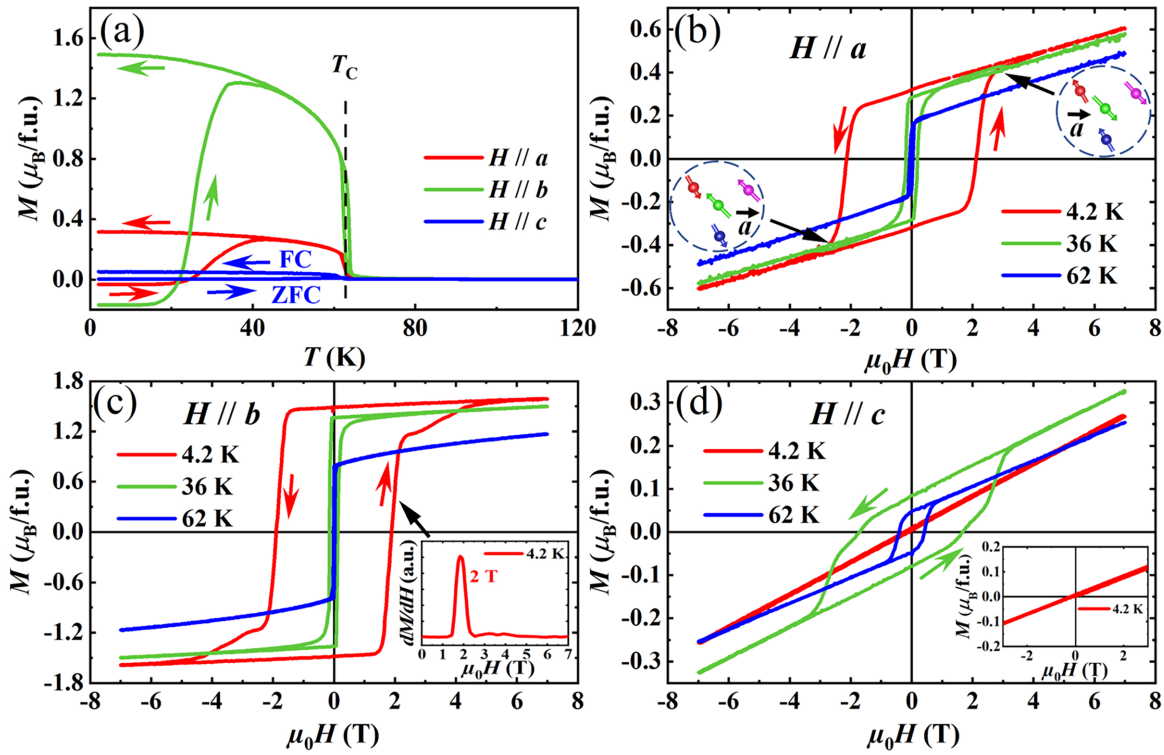

FIG. 2. (a) In both zero-field cooling (ZFC) and field cooling (FC) modes, the temperature dependence of M measured at 0.1 T with the magnetic field along three crystallographic axes. (b)–(d) show the variation of M with magnetic field, in which the magnetic field is applied along the a, b, and c axes, respectively; the magnetic field sweep directions are indicated by the arrows. The inset of (b) displays the spin configurations of Co ions projected onto the ab plane at 4.2 K. The inset of (c) shows the dM/dH-H at 4.2 K. The inset of (d) shows the low-field region M-H curve at 4.2 K.

Magnetic Field Center. The duration of the pulsed magnetic field for the measurements of magnetization (M), polarization (ΔP), and magnetostriction ($\Delta L/L$) is 30–100 ms. The magnetization of the pulsed high magnetic field is measured by conventional induced sensing coil methods. The polarizations were measured with the electric field along the c axis, and the samples were poled with the bias electric field of $E = \pm 160$ kV/m from 80 K to the selected temperatures. Before the polarization measurement, the circuit is shorted for 30 min to release the space charge of the sample. In order to accurately analyze the coupling of the polarization and magnetic moment and how they change with the applied magnetic field, both "M" and "ΔP" are simultaneously measured using the experimental configuration shown in Fig. S1 (in the Supplemental Material [34]).

III. RESULTS AND DISCUSSIONS

The XRD pattern shows that the CBCO single-crystal samples are oriented along the a axis and have good crystallinity [see Fig. 1(a)]. At room temperature, CBCO is an orthorhombic noncentrosymmetric crystal structure (space group $Pbn2_1$) [35]. As shown in Fig. 1(b), the crystal structure of CBCO consists of alternating triangular (T) and kagome (K) layers of CoO_4 tetrahedra stacked along the c axis, and the CoO_4 tetrahedra in the ab plane form the corrugated K layer [26]. As shown in Figs. 1(c) and 1(d), there are four symmetry inequivalent cobalt sites in the unit cell [the dashed rectangle represents the unit cell in Fig. 1(c)]: the Co1, Co2, Co3, and Co4 ions are labeled with green, blue, red, and pink balls, respectively. The spin at the Co4 site is almost parallel to the b axis and antiparallel to the net magnetic moment direction of the "Co2-Co3" zigzag chain. The magnetic moment direction of the Co1 ion is also approximately antiparallel to that of the "Co2-Co3" zigzag chain, which leads to a ferrimagnetic configuration [28,36,37], and the net magnetic moments tend to align along the b axis as shown in Figs. 1(c) and 1(d).

The temperature dependence of M of the CBCO single crystal is shown in Fig. 2(a), in which the applied magnetic field (H) is 0.1 T and the temperature ranges from 2 to 120 K. At $T_C \sim 62$ K, obvious transitions are observed at the magnetic field along all three principal axes. Above T_C, the curves of field cooling (FC) and zero-field cooling (ZFC) coincide well, and no hysteretic behavior is found. Below the temperatures 44 K ($H \parallel a$), 44 K ($H \parallel b$), and 62 K ($H \parallel c$), the ZFC curves deviate from the FC ones, which might result from the magnetic frustration in CBCO [31,32]. Below T_C, the value of the magnetization of the FC curves of M_b is significantly larger than that of M_a and M_c, indicating that CBCO has obvious magnetic anisotropy, and the b axis is the magnetization easy axis [38,39].

Figures 2(b), 2(c), and 2(d) respectively show the variation of M with the magnetic field. Before magnetization measurements, the samples were cooled down to the selected temperatures in zero field, and then the magnetic hysteresis loop was measured in two succession field scanning processes of (i) 7 T→0 T→−7 T and (ii) −7 T→0 T→7 T. As shown in Fig. 2(b), at 4.2 K, in the process (i), M decreases

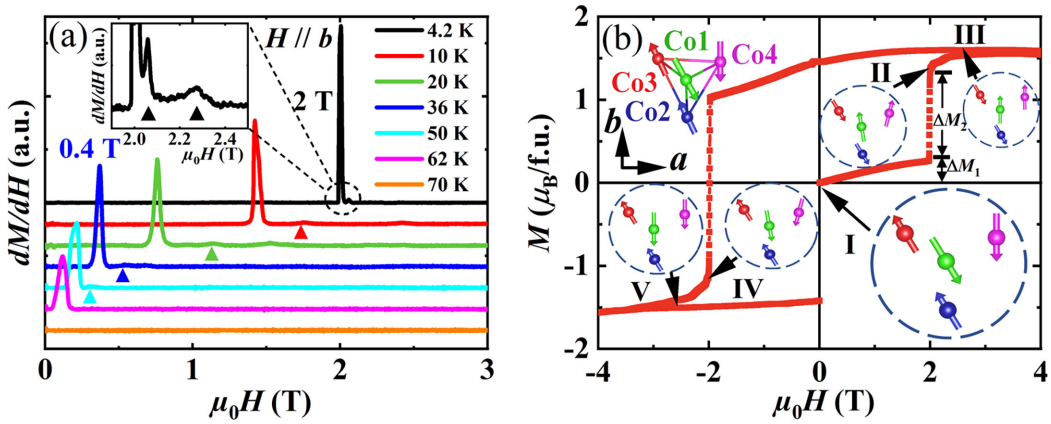

FIG. 3. (a) The magnetic field dependence of dM/dH measured with the pulsed magnetic field along the b axis. The triangle symbols indicate the metamagnetic transitions. (b) The M vs magnetic field curve in the low-field region and spin configuration of Co ions. The pulsed magnetic field magnetization curve is calibrated with superconducting quantum interference device data.

linearly as the magnetic field changes from 7 T to a negative magnetic field, and a transition is observed at the critical field $\mu_0 H_a = -2.2$ T (the critical magnetic field is determined by the maximum value of dM/dH). As the magnetic field further decreases to -7 T, the value of the M decreases linearly, indicating ferrimagnetic behavior. In the process (ii), M changes linearly as the magnetic field increases from -7 to 2.2 T, and the magnetic transition is observed at 2.2 T. As the magnetic field further increases to 7 T, M increases linearly again, indicating robust ferrimagnetic behavior. With the increase of temperature, the transition fields decrease to the lower magnetic field region, where the critical field at 36 and 62 K is 0.2 and 0.05 T, respectively. As shown in Fig. 2(b), at 4.2 K and above the critical field, the magnetic moment M_a is about 0.45 μ_B /f.u. (3 T), which is much lower than that of the theory saturation 14 μ_B/f.u. [28]. In order to understand the smaller magnetic moment, a possible spin configuration of the Co ions is assumed as shown in the inset of Fig. 2(b), which will be explained in detail in the following section.

Based on neutron diffraction, Omi *et al.* propose that the CBCO crystal contains three kinds of trigonally twinned domains rotated by $\pm 60^\circ$ about the c axis [9,10]. That is, the twinned domains with three different b-axis orientations are formed reflecting the trigonal structure. The "domain" mentioned in this paper is the twinned domains that form three different b-axis orientations. Each domain is almost identical and responds independently to the external magnetic field [9,16]. As the magnetic field increases along the a axis, the spins are canted to the magnetic field direction as shown in the upper right inset of Fig. 2(b), in which the experimental result M_a is 0.45 μ_B /f.u. at 3 T. According to the spin magnetic moment and the spin configuration [28], the net magnetic moment along the a-axis direction is about 0.60 μ_B/f.u., which is close to our experimental results. For the magnetic field along the b axis as shown in Fig. 2(c), at 4.2 K and with the magnetic field increase from -7 to 7 T, the M increases from -1.60 μ_B/f.u. to 1.60 μ_B/f.u. At 2 T, a significant magnetic transition is observed. At 4.2 K and 7 T, the magnetization M_b is 1.60 μ_B/f.u.; the experimental results show that even though the magnetic field is along the easy axis, b axis, the maximum M_b at 7 T is also smaller than the saturation value 14 μ_B/f.u. [28], indicating robust ferrimagnetic behavior in CBCO. With increasing temperature, the critical magnetic fields decrease; the critical fields are 2 and 0.14 T at 4.2 and 36 K, respectively. The magnetic hysteresis loop is almost indistinguishable at 62 K. The metamagnetic transitions at 4.2 K may be related to the increase of spin collinearity (noncollinear to collinear realignment) [9,40]. Figure 2(d) shows the variation of M with magnetic field along the c axis, in which no obvious hysteresis is observed at 4.2 K. At higher temperatures, at 36 and 62 K, phase transitions are observed at the critical fields of 2.7 and 0.5 T, respectively, which are similar to those previously reported [20,22].

A pulsed high magnetic field with high-field sweeping rate is a powerful tool to explore the field-induced magnetic transition. Due to the easy axis being along the b-axis in CBCO, the magnetization, polarization, and magnetostriction are mainly measured along the b axis in this study. Figure 3(a) shows the magnetic field dependence of dM/dH under the pulsed magnetic field at various temperatures. The magnetization curves with the magnetic field along other axes are shown in Fig. S2(a) (see the Supplemental Material). At 4.2 K, three peaks are observed at 2.00, 2.06, and 2.28 T, respectively [see the inset of Fig. 3(a)], in which the peak at 2 T may result from the transition from multidomain to single domain; the other peaks may relate to the noncollinear to collinear transition of Co ion spins. As the temperature is increased close to $T_C \sim 62$ K, the critical fields gradually shift to the lower magnetic field region. Below $T_C \sim 62$ K, the sample is in a ferrimagnetic state [20], and at higher magnetic fields, the spins of the Co ions may undergo a transition from noncollinear to collinear. This kind of noncollinear to collinear transition was also reported in $CaBaCo_{3.9}Ni_{0.1}O_7$, in which the neutron diffraction studies show that Ni substitution drastically modifies the spin structure from noncollinear to collinear. That is, a transition from a noncollinear ferrimagnetic to a collinear ferrimagnetic spin order, with $\uparrow\uparrow\downarrow\downarrow$ antiferromagnetic ordering in the kagome layer, is observed with substitution [22].

To explore the field-induced magnetic ordering, the magnetization behavior was investigated via pulsed high magnetic field. As shown in Fig. 3(b), the smaller magnetic moment (at 4 T) confirms that the ferrimagnetic state of

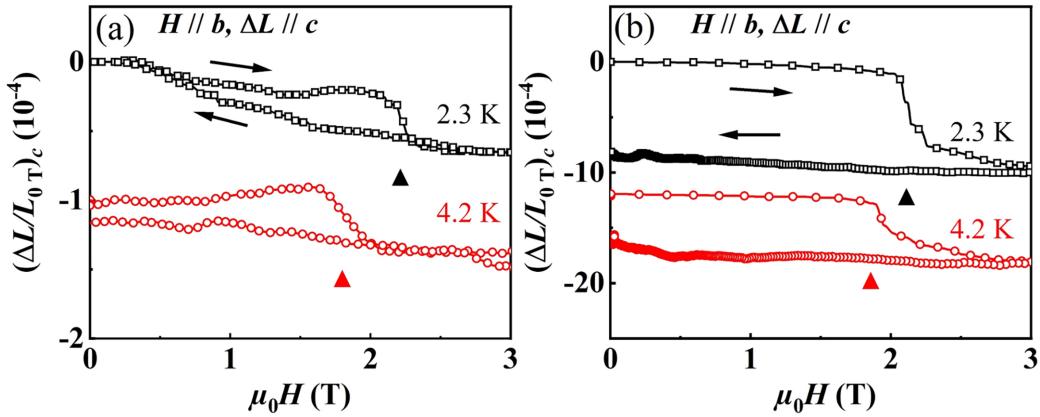

FIG. 4. (a) Magnetostriction measured under static magnetic fields with various temperatures; for clarity, the curve for 4.2 K is shifted down by -1×10^{-4}. The arrows indicate the directions of the magnetic field sweep. (b) Magnetostriction measured with pulsed magnetic fields; the curve at 4.2 K data is shifted down by -12×10^{-4} for clarity. The triangle symbols indicate the critical fields.

the CBCO is robust at low temperatures, and an obvious transition with enhanced hysteresis loop was observed in the *M-H* curve measured by pulsed magnetic field at 4.2 K. It is well known that, in CBCO, the rate of Co^{2+}:Co^{3+} is 1:1, and Co^{2+} ions occupy the Co2/Co3 sites, and the hybridized Co^{3+} ($3d^6$)/Co^{2+} ($3d^7\underline{L}$) ions occupy the Co1/Co4 sites [36,37]. The neutron powder diffraction and bond valence sum calculation [28] show that the magnetic moments of Co1 (2.83 μ_B/Co) and Co4 (2.44 μ_B/Co) ions are larger than that of Co2 (2.04 μ_B/Co) and Co3 (2.05 μ_B μ_B/Co) ions. Based on the spin configuration and their magnetic moments, the observed hysteresis loop can be understood with five different spin configurations [the vignettes of I, II, III, IV, and V in the inset of Fig. 3(b)]. In zero and/or lower magnetic field, the spin configuration of Co ions, in which ferrimagnetic triple chains (Co1 Co2 Co3) run perpendicular to the *ab* plane and are antiferromagnetically coupled with Co4, is shown in vignette I [28]. Below 2 T, with the magnetic field increase, the magnetization increases linearly, indicating the ferrimagnetic characteristic of CBCO. Near 2 T, the net magnetic moment is increased to 0.30 μ_B/f.u. (labeled with ΔM_1). At 2 T, the jump with the change of magnetization 1.00 μ_B/f.u. (labeled with ΔM_2) is observed, which results mainly from the rotation of the magnetic domains in CBCO single crystals. The rotation of the spin and domain can be understood with two continuous processes: (i) In CBCO, $|J_{24}| > |J_{34}| > |J_{23}| > |J_{12}| = |J_{13}| > |J_{14}|$ (where Co2 and Co4 exchange interactions defined as J_{24}, and so on [36]), that is, the antiferromagnetic interaction between Co2 and Co4 is the largest, while the interaction between Co1 and Co4 is the weakest. Under the external magnetic field ($H \parallel b$), Co1 spin is first canted to the magnetic field direction, then the antiferromagnetic coupling between Co1 (Co4) and Co2-Co3 drives the spins of Co2-Co3 ions to tend to antiparallel to the *b* axis and the antiparallel Co2-Co3 in turn causes the spins of Co4 ions to have a deflection from the *b* axis. (ii) At the critical field $\mu_0 H_b = 2$ T, the multidomain state is completely transformed into a single domain state (the spin configuration of Co ions as shown in vignette II), and with the net magnetic moment of 1.30 μ_B/f.u. When the magnetic field further increases to more than 2 T, the spins of the Co1 and Co4 ions firstly experience an arrangement from noncollinear to collinear, and a metamagnetic transition occurs, and the collinearity of Co ion (Co1, Co2, and Co3) spins increases along the *b* axis, as shown in vignette III. The net magnetic moment increases to 1.60 μ_B/f.u. at the magnetic field of 3 T, which is close to the theory calculated value (1.58 μ_B/f.u.) of the spin configuration III [28]. With the further increase of the magnetic field, the magnetization curves show a magnetization plateau due to the robust ferrimagnetic characteristic of CBCO. In the field-decreasing branch, the *M* slightly decreases below 2 T, which might result from the recovery of the noncollinear spins of Co1 and Co4 ions. At -2 T (the negative magnetic field), a jump with the change of the magnetization 2.00 μ_B/f.u. (from 1.00 μ_B/f.u. to -1.00 μ_B/f.u.) is observed, indicating that the magnetic domains are reversed under a reverse magnetic field $\sim$2 T. With the magnetic field changing from -2 to -4 T, the spin configuration changes from vignette IV to vignette V; the situation is similar to that of the field-increasing branch, and the spins of Co1 and Co4 change from noncollinear to collinear. Similarly, *M* weakly decreases when the magnetic field changes from -4 T to 0, probably due to the noncollinear recovery of the spins of the Co1 and Co4 ions.

In order to obtain an overall picture of the dynamics of magnetostriction induced by magnetic ordering in CBCO, the magnetostriction $(\Delta L/L)_c$ at selected temperature was measured using both static [Fig. 4(a)] and pulsed magnetic fields [Fig. 4(b)], in which the magnetostriction is measured along the *c* axis $(\Delta L/L)_c$ and with $H \parallel b$. Here, the sample was cooled down to selected temperatures in zero field before measurements. To exclude the effect of low-temperature magnetoresistance of the strain gauge on the experimental results, the magnetostriction measurement and analysis process involve subtracting the resistance signal of the strain gauge without a sample, in which the same experimental conditions are guaranteed. At 2.3 K, as shown in Fig. 4(a), a transition is observed around 2.2 T. With the increasing magnetic field, the magnetostriction undergoes a significant decrease at the critical magnetic fields. In the field-decreasing branch, the magnetostriction does not exhibit a sudden increase when the magnetic field decreases to less than the critical fields.

Instead, the magnetostriction gradually returns to its initial position. At a higher temperature of 4.2 K, the transition field moves to near 2 T, and the $(\Delta L/L)_c$ is slightly weakened.

Similarly, at the critical field ∼2 T, a transition is also observed at the magnetization curves measured by pulsed magnetic fields as shown in Fig. 3, evidencing the coupling between the field-induced magnetic ordering and lattice distortion [9,15].

As shown in Figs. 4(a) and 4(b), the magnetostriction at low temperatures shows an obvious discrepancy compared to that reported around T_C in the previous paper, suggesting that spin-lattice coupling is influenced by thermal energy [27]. The lattice vibrations activation by the temperature might be damped at lower temperatures, which may show a pinning effect on the field-induced ordering of the spins in CBCO due to spin-lattice coupling in the lower temperatures. Thus, the lower-temperature magnetostriction measurements may reveal more about the intrinsic nature of spin-lattice coupling. To investigate the correlation between the magnetic order and magnetostriction, the $(\Delta L/L)_c$ was measured in pulsed high magnetic fields and lower temperatures. For $H \parallel b$ and at 2.3 K, as shown in Fig. 4(b) a steep decline in magnetostriction is observed at nearly 2.2 T and then slowly decreases to -10×10^{-4}. At 4.2 K the magnetostriction transition field is observed at 2 T with the magnetostriction -6.3×10^{-4}, and the critical field is consistent with the critical magnetic field of the field-induced magnetic ordering shown in Fig. 3. With increasing temperature, the $(\Delta L/L)_c$ decreases and the corresponding transition field moves towards lower fields. Similar to the magnetostriction measured under static magnetic fields, there is a noticeable abrupt change at critical field, along with a longer tail. Considering the spin configuration shown in Fig. 3(b), we assume that the steep decline in magnetostriction mainly results from the rotation of magnetic domains, and the longer tail is related to the increase of the collinearity of the spin of Co1 and Co4 ions. The similar magnetic field dependence of both magnetostriction and magnetization proves the existence of strong spin-lattice coupling [27]. On the other hand, the magnetostriction variation measured under the pulsed magnetic field [Fig. 4(b)] is significantly larger than that under static magnetic field [Fig. 4(a)]. We suppose that this disparity is due to the different rates of magnetic field sweep; the rate of the pulsed magnetic field is $\sim 0.5 \times 10^3$ T/s, which is about five orders of magnitude higher than that of the static magnetic field. The fast change in magnetic field induces a magnetic ordering of the Co ions, which in turn affects the distortion of the lattice, making the magnetostriction results more pronounced. In addition, the deviation of the magnetostriction curve in the field-increasing and field-decreasing branches may be related to the presence of lattice relaxation. At a fixed temperature, the magnetostriction behavior is manifested as a macroscopic lattice shrinks with the increasing magnetic field. Similarly, we have investigated the $(\Delta L/L)_b$ of the b axis and the results show that the magnetostriction behavior is reversed (see Fig. S3 in the Supplemental Material).

To understand the magnetostriction and its dynamic behavior, we reconsider the magnetic order and magnetic domain structure of CBCO. When $H_b > 0$, three twinned domains with different b-axis orientations tend towards the magnetic field direction (b axis) and are accompanied by contraction of the lattice c axis due to exchange striction [16]. The magnetic order can further polarize the orbitals via the second-order spin-orbit interaction, which leads to a strong coupling between spin and lattice. That is, the magnetic field induces the change of the Co-O-Co chain in the c axis, which is the possible source of the observed negative magnetostriction.

In CBCO, the observed $(\Delta L/L)_c$ is attributed to the exchange striction between Co ions [16,26,41], in which the change of the field-induced spin configuration of Co ions leads to the change of the $(\Delta L/L)_c$. To investigate the dynamic behavior of the exchange striction, the $(\Delta L/L)_c$ and M are measured under pulsed magnetic fields (shown in Fig. 5). In this study, two pulsed magnetic fields with different time intervals (Δt) are applied to explore the coupling between the spin and lattice. In particular, the relaxation time between the field-induced magnetic moment flopping and the response in $(\Delta L/L)_c$ is investigated by varying the time interval Δt, in which the duration of the pulsed magnetic field is 70 ms, and the time interval between two pulsed magnetic fields is adjusted from 10 to 710 ms.

As shown in Fig. 5(a), at 4.2 K and below 2 T, with the increase of the magnetic field, the magnetostriction $(\Delta L/L)_c$ decreases slightly. In the magnetic region of 2–3 T, an enhanced decrease of the $(\Delta L/L)_c$ is observed; then, when the magnetic field further increases to 20 T, a smooth decrease tail is observed in the magnetostriction curve. The change of the $(\Delta L/L)_c$ may result from the magnetic domain rotation and the longer tail may relate to the increase of spin collinearity. Magnetization measurements under the pulsed magnetic field show that when the magnetic field is along the b axis, the maximum M_b at 20 T is about 1.75 μ_B/f.u., which is much smaller than the saturation value 14 μ_B/f.u. [28]. The magnetostriction undergoes a significant abrupt change at the critical magnetic field (∼2 T) of the magnetization curve, confirming the presence of spin-lattice coupling in CBCO. In order to investigate the dynamic behavior of $(\Delta L/L)_c$, the magnetostriction recovery is measured with a multipulsed magnetic field. In this paper, we define the recovery as $\Delta L'/L'$, where $\Delta L'$ and L' are shown in Fig. 5(b); the $\Delta L'/L'$ shows the recovery of the $(\Delta L/L)_c$ after the time interval Δt. At 2.3 K, as the Δt changes from 10, 220, 570 to 710 ms, the lattice recovery $\Delta L'/L'$ changes from 13%, 60%, 73%, to 76%, respectively. The longer the time interval Δt, the greater the recovery, which indicates that the relaxation time of the lattice recovery might be longer than the time of the interval Δt, such as 710 ms. In CBCO, the ferrimagnetic structure emerges below $T_C \sim 62$ K, which is accompanied by one of the largest magnetic-order induced polarizations [15,20]. In order to study the change of $(\Delta L/L)_c$ at lower temperature, it is necessary to use high sweep rate pulsed magnetic fields. At 2.3 K, the magnetic field directly drives the spin of the Co ions (and/or magnetic domains) to the magnetic field direction. As shown in Fig. 5(c), in the first pulsed magnetic field, the magnetization behavior is similar to that shown in Figs. 2(c) and 3(b), and an obvious hysteresis is observed. In contrast to the first magnetization curve, there is no noticeable hysteresis in the consecutive (second, third, and fourth) positive pulsed magnetic fields, which indicates that the contribution resulting from the rotation of the magnetic domain is pinned

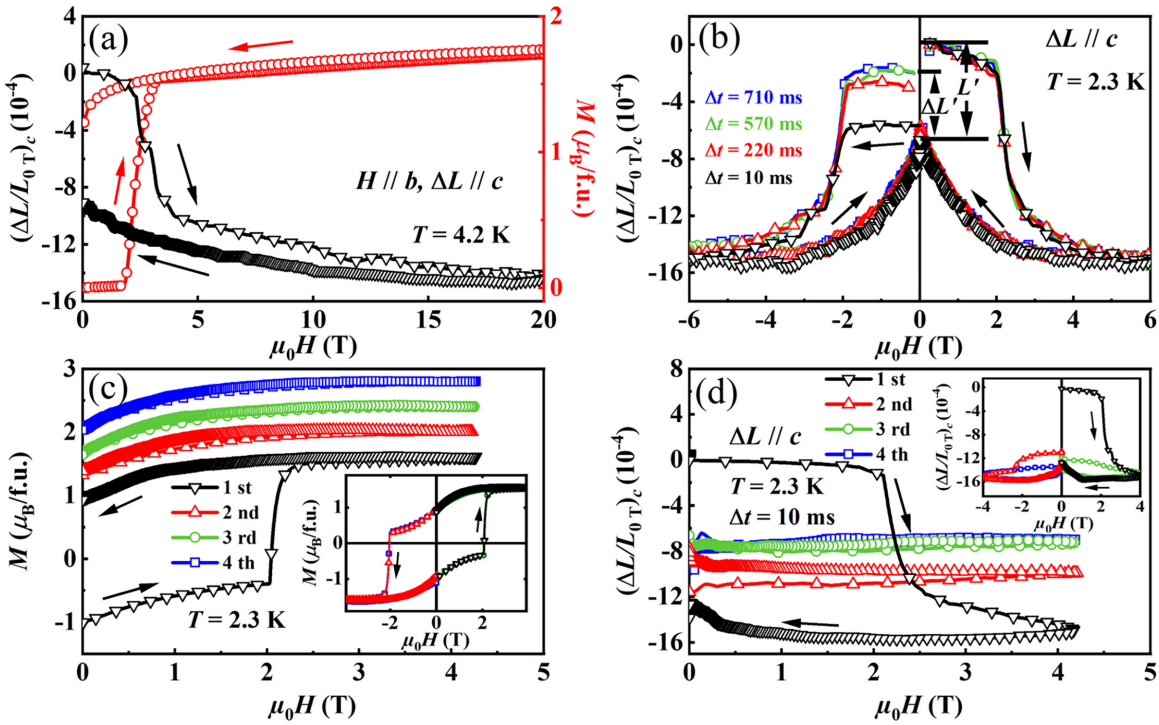

FIG. 5. (a) Magnetic field dependence of magnetostriction and M measured under pulsed magnetic field up to 20 T, where the magnetic field is along the b axis, and ΔL is along the c axis. (b) Magnetic field dependence of magnetostriction $(\Delta L/L)_c$ measured by two continuous pulsed magnetic fields with four different time intervals Δt. Arrows denote the directions of the pulsed magnetic field. (c) The magnetic field dependence of the M measured under four continuous positive pulsed magnetic fields with $\Delta t = 10$ ms; the curves for the second to fourth are shifted up by various magnitudes: 0.4, 0.8, and 1.2 μ_B/f.u. The inset shows the M-H curves measured with four alternating positive and negative pulsed magnetic fields. (d) The magnetic field dependence of the magnetostriction measured under four continuous positive pulsed magnetic fields with $\Delta t = 10$ ms. The inset shows the magnetostriction measured with four alternating positive and negative pulsed magnetic fields.

even though the magnetic field is reduced to zero. However, the magnetic hysteresis loops are recovered in measurements with four alternating positive and negative continuous pulsed magnetic fields [as displayed in the inset of Fig. 5(c)], which indicates that the magnetic domain can be driven by a critical magnetic field ∼2 T. On the other hand, the magnetization results also indicate that the spins of the Co ions rapidly undergo reorientation under the magnetic field, and do not show obvious hysteresis behavior. However, as shown in Fig. 5(b) the incomplete recovery of the magnetostriction $(\Delta L/L)_c$ is observed in the magnetostriction results, which suggests the presence of lattice relaxation.

To explore the memory and training behavior of the magnetostriction $(\Delta L/L)_c$, the $(\Delta L/L)_c$ was measured under four consecutive positive pulsed magnetic fields (labeled with first, second, third, and fourth) with the same time interval of 10 ms. As shown in Fig. 5(d), at 2.3 K, in the first pulse, the magnetostriction behavior is similar to that shown in Fig. 4(b), and an obvious decline is observed around 2.2 T. Compared with the first magnetostriction curve, the magnetostriction gradually decreases under successive (second, third, and fourth) positive pulsed magnetic fields. Compared with Fig. 5(c), at 2.2 T, the steep decline of the magnetostriction in the first pulse is related to the deflection of the magnetic domains. Above 2.2 T, the smaller magnetostriction in the seond pulse is closely related to the lattice relaxation. In order to confirm the different effects between the rotation of the domain and noncollinear to collinear behavior of the spin on the magnetostriction behavior, magnetostrictive measurements were performed using four continuous pulses with a time interval of 10 ms, in which the polarity of the magnetic field was in the order of positive, negative, positive, and negative, marked as first, second, third, and fourth, respectively. As shown in the inset of Fig. 5(d), the domain contribution to $(\Delta L/L)_c$ is always observed due to the field-induced rotation of magnetic domains at 2.2 T (or −2.2 T). Under the pulsed magnetic field from second, third, to fourth, the recovery of $(\Delta L/L)_c$ decreases from 22%, 14%, to 5%, which suggests that the magnetostriction is partially pinned in the training process due to the shorter time interval.

To understand the coupling between spin and lattice, the measurements of the ΔP_c, $(\Delta L/L)_c$, and M are summarized together, as shown in Fig. 6. Similar critical fields demonstrate that the magnetostriction $(\Delta L/L)_c$ is related to field-induced magnetic ordering, that is, spin-lattice coupling exists in CBCO. Qualitatively, the stronger the spin-lattice coupling, the faster the lattice responds to changes in the field-induced magnetic moment. Considering the strength of the interactions between Co ions, $|J_{24}| > |J_{34}| > |J_{23}| > |J_{12}| = |J_{13}| > |J_{14}|$ [36], when the magnetic field is applied to the ferrimagnetic phase, the net magnetic moments of the three domains deflect to the magnetic field direction as possible; in the process, the spin of the Co1 ion is also firstly driven to the direction of the magnetic field, which leads to the increase of the

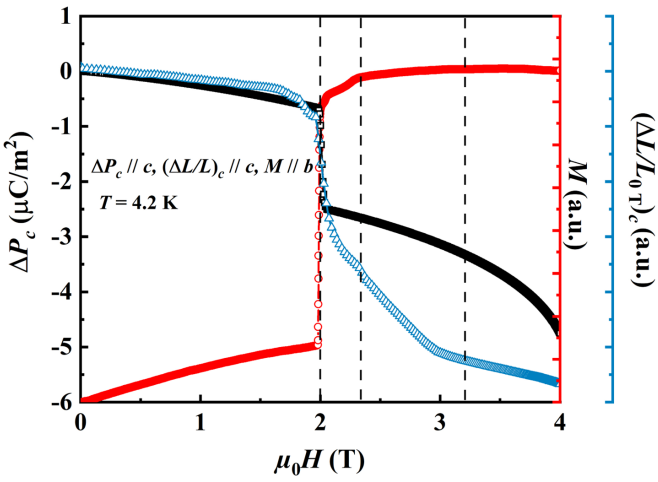

FIG. 6. The magnetic field dependence of the polarization ΔP_c, magnetostriction $(\Delta L/L)_c$, and magnetization M measured at 4.2 K.

magnetization with magnetic fields. At 2 T, the ferrimagnetic multidomain changes to single domain, which results in a magnetization jump of 1.30 μ_B/f.u. As the magnetic field increases further, the spins of the Co1 and Co4 change from noncollinear to collinear. Considering the spin-lattice coupling and exchange striction, in the presence of stronger interactions between the spin and lattice, the lattice is forced to distort to release the stress potential energy. In addition, with the magnetic field decreasing (in the field-decreasing branch), a collinear to noncollinear arrangement of the spin of Co1 and Co4 ions is accompanied in CBCO. The noncollinear to collinear behavior was reported in Ni-doped CBCO [22]. In $CaBaCo_{4-x}Fe_xO_7$, a mean-field approach using Monte Carlo simulations predicts different magnetic orders based on the relative values of two exchange interactions: within the K layer and between the K and T layers [42]. The relative enhancement of the interaction between the K and T layers leads to a collinear ferrimagnetic arrangement. In this research, the different lattice relaxation times under continuous positive and negative pulsed magnetic fields are mainly dominated by the domain rotation time in CBCO [43,44]. The magnetostriction results measured under multipulse [as shown in Fig. 5(d)] further suggest the existence of the dynamics relaxation of spin-lattice coupling.

As shown in Fig. 6, the polarization (ΔP_c) decreases with increasing magnetic field and undergoes a significant abrupt change at 2 T. As the temperature increases, the critical magnetic field shifts towards the lower field region (see Fig. S4 in the Supplemental Material). Below 2 T, as the magnetic field increases, the magnetostriction gradually decreases, accompanied by the Co ion spin deflection. At 2 T, the magnetic field-induced multidomain to single domain transition leads to a sharp change in M. Meanwhile, a sharp jump is also observed in the $(\Delta L/L)_c$ curve, accompanying a sharp decrease in ΔP_c. Above 2 T, the noncollinear to collinear arrangement of the spins of Co1 and Co4 ions is accompanied by a further slow decrease in magnetostriction resulting from exchange striction. The consistent behavior in ΔP_c, $(\Delta L/L)_c$, and M indicates the same origin of the field-induced magnetic ordering (Co spin ordering). Well above the critical field 2 T, the theory magnetization saturation does not reach [15,28], and the polarization and magnetostriction continue to decrease; the evolution of both polarization and magnetostriction driven by magnetic field hints at relaxation of the lattice in CBCO. Combined with the fact that there is a decrease in the magnetostriction at 2 T, it is determined that magnetostriction plays an important role in the polarization process. The polarization dynamic behavior by the induced magnetic field indicates a strong magnetoelectric coupling response in the CBCO.

IV. CONCLUSIONS

In summary, the magnetization, magnetostriction, and polarization behaviors of CBCO are studied, in which the field-induced multidomain to single domain transition and field-induced Co1 and Co4 spin noncollinear to collinear phase transition play an important role. Based on the magnetization and magnetostriction measurements and exchange striction mechanism, the possible metastable magnetic configurations of Co ions in the process of magnetic field change are proposed, in which the magnetostriction is caused by the lattice change of the Co-O-Co chain along the c axis. In the low-temperature region, spin reorientation and lattice relaxation behavior via the action of a multipulse magnetic field further confirms the presence of strong coupling between spin and lattice in CBCO. The results of the magnetostriction measurements further indicate that the strong spin-lattice coupling exhibits obvious dynamic response characteristics to the high sweep rate magnetic fields.

ACKNOWLEDGMENTS

This work is supported in part by the National Key Research and Development Program (Grants No. 2022YFA1602701 and No. 2023YFA1406500).

[1] K. Z. Rushchanskii, S. Kamba, V. Goian, P. Vanek, M. Savinov, J. Prokleska, D. Nuzhnyy, K. Knizek, F. Laufek, S. Eckel, S. K. Lamoreaux, A. O. Sushkov, M. Lezaic, and N. A. Spaldin, A multiferroic material to search for the permanent electric dipole moment of the electron, Nat. Mater. **9**, 649 (2010).

[2] P. Jarillo-Herrero, S. Sapmaz, C. Dekker, L. P. Kouwenhoven, and H. S. Van Der Zant, Electric polarization reversal and memory in a multiferroic material induced by magnetic fields, Nature (London) **429**, 389 (2004).

[3] W. Eerenstein, N. D. Mathur, and J. F. Scott, Multiferroic and magnetoelectric materials, Nature (London) **442**, 759 (2006).

[4] M. Fiebig, T. Lottermoser, D. Meier, and M. Trassin, The evolution of multiferroics, Nat. Rev. Mater. **1**, 16046 (2016).

[5] S. K. Kim, G. S. D. Beach, K. J. Lee, T. Ono, T. Rasing, and H. Yang, Ferrimagnetic spintronics, Nat. Mater. **21**, 24 (2022).

[6] M. M. Vopson, Fundamentals of multiferroic materials and their possible applications, Crit. Rev. Solid State Mater. Sci. **40**, 223 (2015).

[7] S. Lee, M. T. Fernandez-Diaz, H. Kimura, Y. Noda, D. T. Adroja, S. Lee, J. Park, V. Kiryukhin, S. W. Cheong, M. Mostovoy, and J.-G. Park, Negative magnetostrictive magnetoelectric coupling of $BiFeO_3$, Phys. Rev. B **88**, 060103(R) (2013).

[8] N. Aliouane, D. N. Argyriou, J. Strempfer, I. Zegkinoglou, S. Landsgesell, and M. v. Zimmermann, Field-induced linear magnetoelastic coupling in multiferroic $TbMnO_3$, Phys. Rev. B **73**, 020102(R) (2006).

[9] M. Gen, A. Miyake, H. Yagiuchi, Y. Watanabe, A. Ikeda, Y. H. Matsuda, M. Tokunaga, T. Arima, and Y. Tokunaga, Enhancement of giant magnetoelectric effect in Ni-doped $CaBaCo_4O_7$, Phys. Rev. B **105**, 214412 (2022).

[10] V. S. Zapf, V. F. Correa, P. Sengupta, C. D. Batista, M. Tsukamoto, N. Kawashima, P. Egan, C. Pantea, A. Migliori, J. B. Betts, M. Jaime, and A. Paduan-Filho, Direct measurement of spin correlations using magnetostriction, Phys. Rev. B **77**, 020404(R) (2008).

[11] G. Lawes, A. B. Harris, T. Kimura, N. Rogado, R. J. Cava, A. Aharony, O. Entin-Wohlman, T. Yildirim, M. Kenzelmann, C. Broholm, and A. P. Ramirez, Magnetically driven ferroelectric order in $Ni_3V_2O_8$, Phys. Rev. Lett. **95**, 087205 (2005).

[12] L. I. Vergara, J. Cao, N. Rogado, Y. Q. Wang, R. P. Chaudhury, R. J. Cava, B. Lorenz, and J. L. Musfeldt, Magnetoelastic coupling in multiferroic $Ni_3V_2O_8$, Phys. Rev. B **80**, 052303 (2009).

[13] K. Taniguchi, N. Abe, T. Takenobu, Y. Iwasa, and T. Arima, Ferroelectric polarization flop in a frustrated magnet $MnWO_4$ induced by a magnetic field, Phys. Rev. Lett. **97**, 097203 (2006).

[14] T. Kimura, J. C. Lashley, and A. P. Ramirez, Inversion-symmetry breaking in the noncollinear magnetic phase of the triangular-lattice antiferromagnet $CuFeO_2$, Phys. Rev. B **73**, 220401(R) (2006).

[15] V. Caignaert, A. Maignan, K. Singh, C. Simon, V. Pralong, B. Raveau, J. F. Mitchell, H. Zheng, A. Huq, and L. C. Chapon, Gigantic magnetic-field-induced polarization and magnetoelectric coupling in a ferrimagnetic oxide $CaBaCo_4O_7$, Phys. Rev. B **88**, 174403 (2013).

[16] T. Omi, Y. Watanabe, N. Abe, H. Sagayama, A. Nakao, K. Munakata, Y. Tokunaga, and T.-h. Arima, Antiferromagnetic-to-ferrimagnetic phase transition with large electric-polarization change in a frustrated polar magnet $CaBaCo_4O_7$, Phys. Rev. B **103**, 184412 (2021).

[17] S. Yu, C. Dhanasekhar, V. Adyam, S. Deckoff-Jones, M. K. L. Man, J. Madéo, E. L. Wong, T. Harada, M. B. Murali Krishna, K. M. Dani, and D. Talbayev, Terahertz-frequency magnetoelectric effect in Ni-doped $CaBaCo_4O_7$, Phys. Rev. B **96**, 094421 (2017).

[18] S. Bordács, V. Kocsis, Y. Tokunaga, U. Nagel, T. Rõõm, Y. Takahashi, Y. Taguchi, and Y. Tokura, Unidirectional terahertz light absorption in the pyroelectric ferrimagnet $CaBaCo_4O_7$, Phys. Rev. B **92**, 214441 (2015).

[19] N. Lee, C. Vecchini, Y. J. Choi, L. C. Chapon, A. Bombardi, P. G. Radaelli, and S. W. Cheong, Giant tunability of ferroelectric polarization in $GdMn_2O_5$, Phys. Rev. Lett. **110**, 137203 (2013).

[20] Y.-S. Chai, J.-Z. Cong, J.-C. He, D. Su, X.-X. Ding, J. Singleton, V. Zapf, and Y. Sun, Giant magnetostriction and non-saturating electric polarization up to 60 T in the polar magnet $CaBaCo_4O_7$, Phys. Rev. B **103**, 174433 (2021).

[21] C. Dhanasekhar, A. K. Das, A. Das, and A. Venimadhav, Ferroelectricity in $CaBaCo_4O_7$ by light non magnetic Zn doping, J. Phys.: Condens. Matter **32**, 385802 (2020).

[22] C. Dhanasekhar, A. K. Das, R. Singh, A. Das, G. Giovannetti, D. Khomskii, and A. Venimadhav, Switching from pyroelectric to ferroelectric order in Ni-doped $CaBaCo_4O_7$, Phys. Rev. B **96**, 134413 (2017).

[23] H. Iwamoto, M. Ehara, M. Akaki, and H. Kuwahara, Magnetoelectric property in $3d$ transition metal oxide with tetrahedral structure, J. Phys.: Conf. Ser. **400**, 032031 (2012).

[24] R. Oda, R. Kajihara, K. Nishina, M. Akaki, H. Kuroe, and H. Kuwahara, Impurity substitution effect on magnetoelectric properties of $CaBaCo_4O_7$ crystals, Phys. Procedia **75**, 303 (2015).

[25] K. Singh, V. Caignaert, L. C. Chapon, V. Pralong, B. Raveau, and A. Maignan, Spin-assisted ferroelectricity in ferrimagnetic $CaBaCo_4O_7$, Phys. Rev. B **86**, 024410 (2012).

[26] R. D. Johnson, K. Cao, F. Giustino, and P. G. Radaelli, $CaBaCo_4O_7$: A ferrimagnetic pyroelectric, Phys. Rev. B **90**, 045129 (2014).

[27] V. Kocsis, Y. Tokunaga, T. Room, U. Nagel, J. Fujioka, Y. Taguchi, Y. Tokura, and S. Bordacs, Spin-lattice and magnetoelectric couplings enhanced by orbital degrees of freedom in polar multiferroic semiconductors, Phys. Rev. Lett. **130**, 036801 (2023).

[28] V. Caignaert, V. Pralong, V. Hardy, C. Ritter, and B. Raveau, Magnetic structure of $CaBaCo_4O_7$: Lifting of geometrical frustration towards ferrimagnetism, Phys. Rev. B **81**, 094417 (2010).

[29] M. Jaime, A. Saul, M. Salamon, V. S. Zapf, N. Harrison, T. Durakiewicz, J. C. Lashley, D. A. Andersson, C. R. Stanek, J. L. Smith, and K. Gofryk, Piezomagnetism and magnetoelastic memory in uranium dioxide, Nat. Commun. **8**, 99 (2017).

[30] V. Kocsis, Y. Tokunaga, S. Bordács, M. Kriener, A. Puri, U. Zeitler, Y. Taguchi, Y. Tokura, and I. Kézsmárki, Magnetoelectric effect and magnetic phase diagram of a polar ferrimagnet $CaBaFe_4O_7$, Phys. Rev. B **93**, 014444 (2016).

[31] M. M. Seikh, T. Sarkar, V. Pralong, V. Caignaert, and B. Raveau, Dramatic effect of A-site substitution upon the structure and magnetism of the "114" $CaBaCo_4O_7$ cobaltite, Phys. Rev. B **86**, 184403 (2012).

[32] J. Lohr, A. L. Larralde, J. Curiale, R. Sánchez, J. Campo, G. J. Cuello, D. Sheptyakov, L. Keller, M. Kenzelmann, and G. Aurelio, Intermediate magnetic phase of the magnetoelectric compound (Ca, Sr)$BaCo_4O_7$ described with the superspace formalism, Phys. Rev. B **102**, 134406 (2020).

[33] Y. Tokunaga, S. Iguchi, T. Arima, and Y. Tokura, Magnetic-field-induced ferroelectric state in $DyFeO_3$, Phys. Rev. Lett. **101**, 097205 (2008).

[34] See Supplemental Material at http://link.aps.org/supplemental/10.1103/PhysRevB.109.104418 for schematic diagram of simultaneous magnetization and polarization measurement systems under pulsed magnetic fields, as well as the results of magnetostriction and polarization which were used for comparison.

[35] Y. Zou, Z. Qu, L. Zhang, W. Ning, L. Ling, L. Pi, and Y. Zhang, The effect of Al doping on the structure and magnetism in cobaltite $CaBaCo_4O_7$, J. Alloys Compd. **576**, 1 (2013).

[36] S. Chatterjee and T. Saha-Dasgupta, Electronic and magnetic

structure of the mixed-valence cobaltite $CaBaCo_4O_7$, Phys. Rev. B **84**, 085116 (2011).

[37] R. S. Fishman, S. Bordács, V. Kocsis, I. Kézsmárki, J. Viirok, U. Nagel, T. Rõõm, A. Puri, U. Zeitler, Y. Tokunaga, Y. Taguchi, and Y. Tokura, Competing exchange interactions in multiferroic and ferrimagnetic $CaBaCo_4O_7$, Phys. Rev. B **95**, 024423 (2017).

[38] M. Motin Seikh, V. Caignaert, V. Pralong, and B. Raveau, High sensitivity of magnetism of the "114" ferrimagnet $CaBaCo_4O_7$ to stoichiometry deviation, J. Phys. Chem. Solids **75**, 79 (2014).

[39] M. Motin Seikh, T. Sarkar, V. Pralong, V. Caignaert, and B. Raveau, Complex magnetic phase separation induced by Li-doping in multiferroic $CaBaCo_4O_7$, J. Appl. Phys. **113**, 053910 (2013).

[40] Z. A. Kazei, V. V. Snegirev, G. P. Vorob'ev, Y. F. Popov, D. K. Vyalykh, L. P. Kozeeva, and M. Y. Kameneva, Elastic, magnetic, and magnetoelectric properties of the $CaBaCo_4O_7$ multiferroic, J. Exp. Theor. Phys. **123**, 1025 (2017).

[41] A. Ikeda, S. Furukawa, O. Janson, Y. H. Matsuda, S. Takeyama, T. Yajima, Z. Hiroi, and H. Ishikawa, Magnetoelastic couplings in the deformed kagome quantum spin lattice of volborthite, Phys. Rev. B **99**, 140412(R) (2019).

[42] V. Cuartero, J. Blasco, G. Subias, J. Garcia, J. A. Rodriguez-Velamazan, and C. Ritter, Structural, magnetic, and electronic properties of $CaBaCo_{4-x}M_xO_7$ (M = Fe, Zn), Inorg. Chem. **57**, 3360 (2018).

[43] L. Alberts and E. W. Lee, Magnetostriction in antiferromagnetic nickel oxide, Proc. Phys. Soc. **78**, 728 (1961).

[44] J.-C. He, Z. Pan, D. Su, X.-D. Shen, J. Zhang, D.-B. Lu, H.-T. Zhao, J.-Z. Cong, E.-K. Liu, Y.-W. Long, and Y. Sun, Magnetic-field-induced sign changes of thermal expansion in $DyCrO_4$, Chin. Phys. Lett. **40**, 066501 (2023).